Astronomy & Astrophysics manuscript no. paper
(DOI: will be inserted by hand later)

arXiv:astro-ph/0511499v1 16 Nov 2005

On the interpretation of the spectral–energy correlations in long Gamma–Ray Bursts

Nava L.[1,2], Ghisellini G.[1], Ghirlanda G.[1], Tavecchio F.[1], Firmani C.[1,3]

[1] Osservatorio Astronomico di Brera, via Bianchi 46, Merate Italy
[2] Univ. di Milano–Bicocca, P.za della Scienza 3, I–20126, Milano, Italy.
[3] Instituto de Astronomía, U.N.A.M., A.P. 70-264, 04510, México, D.F., México

Received ... / Accepted ...

Abstract. Recently, Liang & Zhang (2005) found a tight correlation involving only observable quantities, namely the isotropic emitted energy $E_{\gamma,\rm iso}$, the energy of the peak of the prompt spectrum $E'_{\rm p}$, and the jet break time $t'_{\rm j}$. This phenomenological correlation can have a first explanation in the framework of jetted fireballs, whose semiaperture angle $\theta_{\rm j}$ is indeed measured by the jet break time $t'_{\rm j}$. By correcting $E_{\gamma,\rm iso}$ for the angle $\theta_{\rm j}$ one obtains the so called Ghirlanda correlation which links the collimation corrected energy E_γ and $E'_{\rm p}$. There are two ways to derive $\theta_{\rm j}$ from $t'_{\rm j}$ in the "standard" scenario, corresponding to an homogeneous or instead to a wind–like circumburst medium. We show that the Ghirlanda correlation with a wind–like circumburst medium is as tight as (if not tighter) than the Ghirlanda correlation found in the case of an homogeneous medium. There are therefore two Ghirlanda correlations, both entirely consistent with the phenomenological Liang & Zhang relation. We then suggest to consider the difference between the *observed* correlations and the ones one would see in the *comoving frame* (i.e. moving with the same bulk Lorentz factor of the fireball). Since both $E_{\rm p}$ and E_γ transform in the same way, the wind–like Ghirlanda relation, which is linear, remains linear also in the comoving frame, no matter the distribution of bulk Lorentz factors. Instead, in the homogeneous density case, one is forced to assume the existence of a strict relation between the bulk Lorentz factor and the total energy, which in turn put constraints on the radiation mechanisms of the prompt emission. The wind–like Ghirlanda correlation, being linear, corresponds to different bursts having the same number of photons.

Key words. Gamma rays: bursts — Radiation mechanisms: non-thermal — X–rays: general

1. Introduction

The correlation between the collimation corrected emitted energy in the prompt phase of GRBs (E_γ) and the peak energy of the νE_ν prompt spectrum ($E_{\rm p}$), the so–called "Ghirlanda" relation, is the fundamental tool for the cosmological use of GRBs.

Its importance calls for a robust and convincing explanation. Possible ideas and interpretations have already been proposed, but requiring some ad hoc assumptions: different authors (Eichler & Levinson 2004; Levinson & Eichler 2005; Yamazaki, Ioka & Nakamura 2004; Toma, Yamazaki & Nakamura 2005) have underlined the importance of viewing angle effects assuming different geometries of the fireball (annular or patchy); while Rees & Meszaros (2005) pointed out that a strict relation between total energy and typical peak frequency can be understood in a easier way if the underlying emission process is thermal, therefore suggesting that dissipative processes in the photosphere of the fireball can increase the thermal (black–body like) photon content of the fireball itself.

The collimation corrected energy E_γ is derived by multiplying the isotropic emitted energy $E_{\gamma,\rm iso}$ by the factor $(1-\cos\theta_{\rm j})$, where $\theta_{\rm j}$ is the semiaperture angle of the jet. To derive it, one must assume the uniform jet model and the density profile of the circumburst medium (e.g. homogeneous or wind–like).

The Ghirlanda correlation has been derived for an homogeneous density (i.e. n constant) and there are a few critical points concerning its derivation which are now under discussion.

Firstly, in this scenario the jet opening angle is (Sari et al. 1999)

$$\theta_{\rm j} = 0.161 \left(\frac{t_{\rm j,d}}{1+z}\right)^{3/8} \left(\frac{n\,\eta_\gamma}{E_{\gamma,\rm iso,52}}\right)^{1/8} \qquad (1)$$

where z is the redshift, η_γ is the radiative efficiency and $t_{\rm j,d}$ is the achromatic break time, measured in days, of the afterglow lightcurve [1]. The efficiency η_γ relates the isotropic kinetic energy of the fireball after the prompt phase, $E_{\rm k,iso}$, to the prompt emitted energy $E_{\gamma,\rm iso}$, through $E_{\rm k,iso} = E_{\gamma,\rm iso}/\eta_\gamma$. This implicitly assumes that $\eta_\gamma \ll 1$ otherwise the remaining

Send offprint requests to: Gabriele Ghisellini
gabriele@merate.mi.astro.it

[1] Here we adopt the notation $Q = 10^x Q_x$, and use cgs units unless otherwise noted.

kinetic energy after the prompt emission is instead $E_{\rm k,iso} = E_{\gamma,\rm iso}(1-\eta_\gamma)/\eta_\gamma$. This efficiency, in principle, could be different from bursts to bursts, but in the absence of any hints of how its value changes as a function of other properties of the bursts and favoured by its low power in Eq.1, one assumes a constant value for all bursts, i.e. $\eta_\gamma = 0.2$ (after its first use by Frail et al. 2001, following the estimate of this parameter in GRB 970508).

Secondly, the density of the circumburst medium n can in principle be estimated through accurate fits to the lightcurves at different frequencies [or, equivalently, fitting the spectral energy distributions (SEDs) at different times], but the fact that the emitted synchrotron spectrum is insensitive to n in the regime of fast cooling makes the n estimates somewhat uncertain. Furthermore, only for a minority of bursts we have enough data to constrain n even in a rather poor way (see e.g. Panaitescu & Kumar 2000, 2001). From this partial information, however, the estimated values of n range from ~ 0.1 to ~ 30 cm^{-3} with a clear preference for an homogeneous density scenario. Wind density profiles are acceptable and even preferred in few cases, in which however one cannot exclude the homogeneous density case. This led to the choice, made by Ghirlanda, Ghisellini & Lazzati (2004, hereafter GGL04) to assume an homogeneous density scenario for all bursts and assign, to all cases in which n was not estimated, a range of possible values of n, from 1 to 10 cm^{-3}, to derive the value of $\theta_{\rm j}$ using Eq. 1, and, more importantly, the associated error. However, if GRBs are expected to originate from the death of very massive stars, the wind density profile appears as the most natural outcome of the final stages of the evolution of the burst progenitor.

These issues on one hand must caution us about the possible scatter of the points in the Ghirlanda correlation, which may well be the results of bursts having a distribution (instead of a single value) of n and η_γ, but on the other hand the extremely small scatter found suggests that, for the considered bursts, these values are indeed clustered in a small range.

In any case, these concerns (i.e. a possible distribution of n and η_γ values) have been completely overcome by the finding, by Liang & Zhang (2005, hereafter LZ05), of a phenomenological and model–independent correlation between $E_{\gamma,\rm iso}$, $E'_{\rm p}$ and $t'_{\rm j}$. By considering 15 GRBs, and a flat Universe cosmology with $\Omega_{\rm M} = 0.28$ and $h_0 = 0.713$, the correlation found by LZ05 takes the form:

$$E_{\gamma,\rm iso,52} = (0.85 \pm 0.21) \left(\frac{E'_{\rm p}}{100\,\rm keV}\right)^{1.94\pm0.17} t'^{-1.24\pm0.23}_{\rm j,d} \quad (2)$$

where primed quantities are calculated in the rest frame of the GRB, i.e. $t' = t/(1+z)$ and $E'_{\rm p} = E_{\rm p}(1+z)$. The scatter of the data points around this correlation is small enough to enable LZ05 to use it for finding constraints to the cosmological parameters.

The main aim of the present paper is to discuss a few steps which we think necessary in order to deepen our understanding of the spectral/energy correlations in GRB, even if we do not claim to arrive to a complete or satisfactory interpretation. The Ghirlanda correlation (although derived earlier than the LZ05 relation) should be considered as a first step towards the explanation of the purely phenomenological LZ05 relation.

The first step is to demonstrate that the LZ05 correlation is equivalent to the Ghirlanda correlation. Secondly, we explore what happens to the Ghirlanda correlation if, instead of an homogeneous medium, we assume that the density is distributed with a r^{-2} wind profile. We demonstrate that the LZ05 is again consistent with this new Ghirlanda–wind correlation.

We then have not one, but two possibilities of relating $E_{\rm p}$ and E_γ, both consistent with the LZ05 correlation. We argue that the new (wind–like) Ghirlanda correlation cannot be easily discarded on the basis of the fit to the afterglow SEDs, which prefer the uniform density case. The present small sample of GRBs does not allow to test the two possibilities, but we mention one test to do so when estimates of the initial bulk Lorentz factor will be available.

We then discuss a third step, pointing out that the observed $E_{\rm p}$ and E_γ are affected by the relativistic motion of the fireball. In the simplest and standard scenario, which assumes that the observer's line of sight is within the jet opening angle and that the jet is homogeneous, $E_{\rm p}$ and E_γ are both boosted by a factor $\sim 2\Gamma$, where Γ is the bulk Lorentz factor of the fireball. Therefore what we see is an *apparent* correlation. Imposing that some correlation (even different from the observed one) exists in the comoving frame allows to put interesting constraints on both the dynamics and the emission processes of bursts.

As part of our effort, we report the updated tables for the relevant parameters used in deriving all the results and correlations discussed in the present paper. We discuss case–by–case the differences and changes of these quantities with respect to previously published papers.

2. The sample

LZ05 found their correlation (Eq. 2) by using 15 bursts. Most of them are the same bursts used by GGL04, but there are some differences in the reported parameters for the common GRBs. Also, since the publication of GGL04 some (primarily spectral) parameters have been updated (as a consequence of refined analysis) and published in the literature. Finally, other bursts have been detected recently, which bring the total number of GRBs with "useful" data (i.e. z, $E_{\rm p}$ and $t_{\rm j}$, excluding upper/lower limits) to 18 (at the time of writing, September 2005). We stress that our sample includes only those bursts with secure measurements of $z, E_{\rm peak}, t_{\rm j}$. Consistency checks of the upper/lower limits can be performed (as shown in GGL04). For these reasons we present in Tab. 1 our sample of 18 GRBs with the relevant input data and corresponding references which represents the most updated collection of published parameters which are relevant for our analysis. We detail in the following all the relevant differences of this table with respect to that reported in GGL04 and LZ05.

Tab. 1 contains all GRBs reported by LZ05 with the exception of GRB 021211, and with the addition of 4 GRBs (GRB 970828, GRB 990705, GRB 041006, GRB 050525). Our exclusion of GRB 021211 is motivated by the extremely uncertain determination of $t_{\rm j}$ due to the scarcity of afterglow data

GRB	z	α	β	Fluence erg/cm^2	Range keV	$E_{\rm p}$ keV	Ref^a	$t_{\rm j}$ days	n cm^{-3}	Ref^b
970828	0.958	–0.70 [0.08]	–2.07 [0.37]	9.6e–5 [0.9]	20–2000	298 [60]	1, 2	2.2 (0.4)	3.0 [2.76]	25, ...
980703	0.966	–1.31 [0.14]	–2.40 [0.26]	2.26e–5[0.23]	20–2000	254 [51]	3, 2	3.4 (0.5)	28 (10)	25, 25
990123	1.600	–0.89 (0.08)	–2.45 (0.97)	3.0e–4 (0.4)	40–700	781 (62)	4, 5	2.04 (0.46)	3.0 [2.76]	26, ...
990510	1.619	–1.23 (0.05)	–2.7 (0.4)	1.9e–5 (0.2)	40–700	161 (16)	6, 5	1.6 (0.2)	0.29 (0.13)	27, 36
990705	0.843	–1.05 (0.21)	–2.2 (0.1)	7.5e–5 (0.8)	40–700	189 (15)	7, 5	1.0 (0.2)	3.0 [2.76]	25, ...
990712	0.433	–1.88 (0.07)	–2.48 (0.56)	6.5e–6 (0.3)	40–700	65 (11)	6, 5	1.6 (0.2)	3.0 [2.76]	28, ...
991216	1.02	–1.23 [0.13]	–2.18 [0.39]	1.9e–4 [0.2]	20–2000	318 [64]	8, 2	1.2 (0.4)	4.7 (3.5)	25, 36
011211	2.140	–0.84 (0.09)	...	2.6e–6 [0.3]	40–700	59 (8)	9, 9	1.56 [0.16]	3.0 [2.76]	29, ...
020124	3.198	–0.87 (0.17)	–2.6 (0.65)	8.1e–6 (0.9)	2–400	93 (27)	10, 11	3.0 [0.4]	3.0 [2.76]	30, ...
020405	0.695	–0.0 (0.25)	–1.87 (0.23)	7.4e–5 [0.7]	15–2000	364 (101)	12, 12	1.67 (0.52)	3.0 [2.76]	12, ...
020813	1.255	–1.05 [0.11]	...	1.0e–4 [0.1]	30–400	212 [42]	13, 14	0.43 (0.06)	3.0 [2.76]	25, ...
021004	2.335	–1.0 (0.2)	...	2.6e–6 (0.6)	2–400	80 (35)	15, 16	4.74 [0.5]	3.0 [2.76]	31, ...
030226	1.986	–0.9 (0.2)	...	5.6e–6 (0.6)	2–400	97 (21)	17, 16	1.04 (0.12)	3.0 [2.76]	32, ...
030328	1.520	–1.14 (0.03)	–2.1 (0.3)	3.7e–5 (0.14)	2–400	130 (14)	18, 16	0.8 [0.1]	3.0 [2.76]	33, ...
030329	0.169	–1.32 (0.02)	–2.44 (0.08)	1.2e–4 [0.12]	30–400	70 (2)	19, 20	0.5 (0.1)	2.2 [0.80]	34, 38
030429	2.656	–1.1 (0.3)	...	8.5e–7 (1.4)	2–400	35 (10)	21, 16	1.77 (1.0)	3.0 [2.76]	35, ...
041006	0.716	–1.37 [0.14]	...	2.0e–5 [0.2]	25–100	63 [13]	22, 22	0.16 (0.04)	3.0 [2.76]	37, ...
050525	0.606	–0.99 (0.11)	...	2.01e–5 (0.05)	15–350	79 (3.5)	23, 24	0.28 (0.12)	3.0 [2.76]	39, ...

Table 1. Input parameters for the bursts of our sample. α and β are the photon spectral indices of the prompt emission spectrum and $E_{\rm p}$ represents the (observed) peak energy of the νF_ν spectrum. When the errors are not given in the original reference, we assumed an average error (values in square brackets), otherwise we list the originally reported error (in round brackets). ^{a}References are given in order for the redshift (z) and for the spectral parameters (α, β, fluence and its energy interval): 1 Djorgovsky et al. 2001; 2 Jimenez et al. 2001; 3 Djorgovsky et al. 1998; 4 Hjorth et al. 1999; 5 Amati et al. 2002; 6 Vreeswijk et al. 2001; 7 Amati et al. 2000; 8 Vreeswijk et al. 1999; 9 Amati 2004; 10 Hjorth et al. 2003; 11 Atteia et al. 2005; 12 Price et al. 2003; 13 Barth et al. 2003; 14 Barraud et al. 2003; 15 Moller et al. 2002; 16 Sakamoto et al. 2005; 17 Greiner et al. 2003a; 18 Rol et al. 2003; 19 Greiner et al. 2003b; 20 Vanderspek et al. 2004; 21 Weidinger et al. 2003; 22 http://space.mit.edu/HETE/Bursts/; 23 Foley et al. 2005; 24 Blustin et al. 2005; ^{b}References are given in order for the observed jet break time $t_{\rm j}$ and for the density n when present: 25 Bloom et al. 2003; 26 Kulkarni et al. 1999; 27 Israel et al. 1999; 28 Bjornsson et al. 2001; 29 Jakobsson et al. 2003; 30 Berger et al. 2002; 31 Holland et al. 2003; 32 Klose et al. 2004; 33 Andersen et al. 2003; 34 Berger et al. 2003; 35 Jakobsson et al. 2004; 36 Panaitescu & Kumar 2002; 37 Stanek et al. 2005; 38 Frail et al. 2005. 39 Blustin et al. 2005

and to the likely "contamination" of a supernova (Della Valle et al. 2003). The value of $t_{\rm j}$ reported by LZ05 (1.4 day, see also Holland et al. 2004) should be considered only as a lower limit to $t_{\rm j}$ (as assumed in GGL04).

For GRBs listed in Tab. 1 which are also present in LZ04 we have the following (minor) differences:

- GRB 011211: the value of $t_{\rm j}$ reported by Jakobsson et al. (2003) is $t_{\rm j} = 1.56 \pm 0.02$ days. This has been derived by fitting the light curve with a broken power law, which very likely severely underestimates the error on this quantity. Note that the χ^2 of the original fit is large. Differently from LZ05, who used the above error, we have set the error to 10% (i.e. the average error on the observed jet break time) of the value of $t_{\rm j}$.
- GRB 020124: the spectral parameters have been updated by Atteia et al. (2005) with respect to the ones assumed by LZ05 from the Sakamoto et al. (2005).
- GRB 020405: for the value of $E_{\rm p}$ listed in Tab. 1 we assume that in the original reference (Price et al. 2003), the authors presented the value E_0 of the Band spectrum. This corresponds to the e–folding energy of the exponential rollover of this model and it allows to derive the peak energy as $E_{\rm p} = E_0(\alpha + 2)$ (where α is the photon spectral index of the low energy power law component of the Band model). Note also that if $\beta = -1.87 \pm 0.23$, as reported in Price et al. 2003, the spectral peak energy is unconstrained within the observational energy band. However, the reported uncertainty (0.23) makes the high energy spectral component consistent with $\beta < -2$. For this reason we assumed the lowest value, i.e.$\beta = -2.1$, to compute the isotropic equivalent energy of this burst.
- GRB 020813: we take the spectral parameters of this GRB from Barraud et al. (2003), while LZ05 use the values reported in the Sakamoto et al. (2005). The reason of our choice is in the fact that, with the $\beta = -1.57 \pm 0.04$ reported by Sakamoto et al. (2005), one could not define the value of $E_{\rm p} = 140 \pm 14$ keV (which instead requires at least $\beta < -2$), which is reported in Sakamoto et al. (2005).

– GRB 021004: the value of $t_{\rm j} = 4.74$ days comes from Holland et al. (2003), and it is the same (as well as the quoted reference) of LZ05. What is different is the error: Holland et al. (2003) report $t_{\rm j} = 4.74^{+0.14}_{-0.80}$ days. LZ05 take 0.14 days as the error in this quantity, while we take 0.5 days to better approximate the (asymmetric) error.
– GRB 030329: We have updated the spectral parameters of this bursts according to the published paper by Vanderspek et al. 2004 (which are somewhat different from those presented in the preprint version of the same article).
– GRB 050525: the prompt emission and the early afterglow detected by the Swift BAT, UVOT and XRT instruments have been recently analyzed by Blustin et al. (2005). In this paper the authors suggest the presence of a jet break in the very early afterglow lightcurve, i.e. $t_{\rm j}$ =0.16 or 0.2 days according to two different model fit (the second value is found including also the data of Klotz et al. 2005, while the first value refers to the Swift data only). On the other hand, Mirabal et al. (2005) noted a jet break time at 0.4 days after trigger, based on a large collection of data (120 frames, still unpublished) taken with the 2.4 MDM meter telescope. Note also that the fit leading to $t_{\rm j} = 0.2$ days assumes that the optical afterglow has a "jump" in its flux, but that thereafter continues to decay normally. In other words, this "discontinuity" is not treated as a "bump" in the lightcurve (as often seen in other bursts) which would have implied that the afterglow is composed by two contributions (the normal afterglow plus the re-brightening component). Fitting with this model would result in a larger value of $t_{\rm j}$. While waiting for a joint fit with all the data available, and also with different models, we decided to use $t_{\rm j} = 0.28 \pm 0.12$ days: this value is intermediate between the Blustin et al. values and the Mirabal et al. value, with an error which encompasses all values.

In Tab. 2 we report the values of the rest frame peak energy $E'_{\rm p}$ and of the isotropic equivalent energy $E_{\gamma,{\rm iso}}$. The values of $E_{\gamma,{\rm iso}}$ have been taken directly from Amati et al. (2002) in the case of GRBs detected by $Beppo$Sax and listed in that paper, but we converted these values to our cosmology (i.e. we use $h = 0.7$ while Amati et al. 2002 used $h = 0.65$).

Tab. 1 and Tab. 2 are the updated version of the tables presented in GGL04 which were composed by 15 "usable" GRBs. With respect to that paper, our present sample of 18 GRBs comprises 3 new GRBs (GRB 021004, GRB 041006 and GRB 050525) for which z, $E_{\rm p}$ and $t_{\rm j}$ have been published and some of the parameters have changed due to updates which appeared in the literature.

– GRB 991216: the value of the density $n = 4.70^{+6.8}_{-1.8}$ was estimated by Panaitescu & Kumar (2002). We have here assumed a symmetric error equal to the logarithmic average, and taken $n = 4.7 \pm 3.5$. This differs slightly from what assumed in GGL04 ($n = 4.7 \pm 2.3$).
– GRB 011211: we changed the reference for the spectral parameters, which is Amati (2004), and not Amati et al. 2002 as given in GGL04. We recalculated the value of $E_{\gamma,{\rm iso}}$ with $h = 0.7$.
– GRB 020124: we updated the spectral parameters, now taken from Atteia et al. (2005). The main difference concerns $E_{\rm p} = 120$ keV, instead of the value of 93 keV reported in GGL04.
– GRB 030226 and GRB 030328: we now use the spectral parameters reported in Sakamoto et al. (2005) (instead of Atteia 2003) and the recalculated $E_{\gamma,{\rm iso}}$.
– GRB 030329: as mentioned above, we updated the spectral parameters according to the published paper by Vanderspek et al. 2004. The listed value of $n = 2.2$ cm^{-3} comes from Frail et al. 2005 (GGL04, instead, quoted $n = 1$ cm^{-3}): the associated error encompasses the three possible values listed in Tab. 2 of Frail et al. 2005.
– GRB 030429: we updated the spectral parameters with Sakamoto et al. (2005) instead of those assumed in GGL04 which were taken from the Hete-2 web page.

3. The spectral–energy correlations

With the updated sample of 18 GRBs reported in Tab. 1 we first refit the empirical LZ05 correlation among $E_{\gamma,{\rm iso}}$, $E'_{\rm p}$ and $t'_{\rm j}$. We also give the updated version of the Ghirlanda correlation (GGL04 and Ghirlanda et al. 2005) in the case of a homogeneous density profile. Finally we present the Ghirlanda correlation in the case of a wind density profile.

3.1. The Liang–Zhang correlation revisited

The method used by LZ05 to find the correlation between $E_{\gamma,{\rm iso}}$, $E'_{\rm p}$ and $t'_{\rm j}$ is a multivariate linear regression. The significance of the multivariate regression is estimated through the F–test and through the Spearman $r_{\rm s}$ coefficient between $\log E_{\gamma,{\rm iso}}$ calculated through Eq. 2 and the same quantity directly calculated through

$$E_{\gamma,{\rm iso}} = \frac{4\pi d_L^2 S_\gamma k}{1+z} \qquad (3)$$

where d_L is the luminosity distance, S_γ the γ–ray fluence in the observed energy band, k is the bolometric correction factor needed to find the energy emitted in a fixed energy range (here, 1–10000 keV) in the rest frame of the source.

We have used a different method, which enable us to weight the multidimensional fit for the errors on the three independent variables $E_{\gamma,{\rm iso}}$, $E'_{\rm p}$ and $t'_{\rm j}$. By extending to the three dimensional space the procedure for the fit of a straight line to data with errors on two coordinates (Press et al. 1999) we use the χ^2 statistics to find the best fit.

Assuming a $\Omega_{\rm M} = 0.3$ and $h = \Omega_\Lambda = 0.7$ cosmology, we find

$$E_{\gamma,{\rm iso},53} = (1.12\pm0.11) \left(\frac{E'_{\rm p}}{295\,{\rm keV}}\right)^{1.93\pm0.17} \left(\frac{t'_{\rm j}}{0.51{\rm d}}\right)^{-1.08\pm0.17} \qquad (4)$$

with a reduced $\chi^2_{\rm r} = 1.49$. The 3D plot of the data points in the $E_{\gamma,{\rm iso}}$, $E'_{\rm p}$ and $t'_{\rm j}$ space and the best fit plane as defined by Eq. 4 are represented in Fig. 1. Similarly to what has been done in 2D (GGL04) we can define the scatter of the data points around the best fit plane through their distance computed perpendicular to

GRB	$E'_{\rm p}$ keV	$E_{\gamma,\rm iso}$ erg	$\theta_{\rm j}$ deg	E_γ erg	$E_{\gamma,\rm n=3}$ erg	$\theta_{\rm j,w}$ deg	$E_{\gamma,\rm w}$ erg
970828	583 [117]	2.96e53 [0.35]	5.91 ± 0.79	1.57e51 (0.46)	...	3.40 (0.19)	5.21e50 (0.84)
980703	499 [100]	6.9e52 (0.82)	11.02 ± 0.80	1.27e51 (0.24)	7.29e50 (1.20)	5.45 (0.26)	3.12e50 (0.48)
990123	2031 (161)	2.39e54 (0.28)	3.98 ± 0.57	5.76e51 (1.78)	...	1.84 (0.12)	1.24e51 (0.22)
990510	422 (42)	1.78e53 [0.19]	3.74 ± 0.28	3.80e50 (0.69)	6.80e50 (0.98)	3.31 (0.14)	2.98e50 (0.40)
990705	348 (28)	1.82e53 (0.23)	4.78 ± 0.66	6.33e50 (1.92)	...	3.20 (0.19)	2.84e50 (0.50)
990712	93 (16)	6.72e51 (1.29)	9.47 ± 1.20	9.16e49 (2.90)	...	8.75 (0.51)	7.82e49 (1.76)
991216	642 [129]	6.75e53 [0.81]	4.44 ± 0.70	2.03e51 (6.79)	1.81e51 (0.50)	2.36 (0.21)	5.72e50 (1.24)
011211	185 (25)	5.4e52 (0.6)	5.38 ± 0.66	2.38e50 (0.64)	...	4.24 (0.16)	1.48e50 (0.20)
020124	390 [113]	2.61e53 (0.18)	5.07 ± 0.64	1.02e51 (0.27)	...	3.13 (0.12)	3.90e50 (0.40)
020405	617 [124]	1.25e53 [0.13]	6.27 ± 1.03	7.48e50 (2.58)	...	4.08 (0.34)	3.17e50 (0.63)
020813	478 [95]	5.78e53 [0.58]	2.8 ± 0.36	6.89e50 (1.88)	...	1.85 (0.08)	3.00e50 (0.40)
021004	267 (117)	3.38e52 (0.78)	8.47 ± 1.06	3.69e50 (1.25)	...	6.20 (0.40)	1.98e50 (0.52)
030226	290 [63]	5.43e52 (0.68)	4.71 ± 0.58	1.84e50 (0.51)	...	3.88 (0.17)	1.24e50 (0.19)
030328	318 [33]	3.68e53 [0.37]	3.58 ± 0.45	7.18e50 (1.93)	...	2.35 (0.10)	3.09e50 (0.40)
030329	82 (2)	1.62e52 [0.16]	5.69 ± 0.50	7.99e49 (1.62)	8.63e49 (1.56)	5.52 (0.31)	7.51e49 (1.13)
030429	128 [26]	1.42e52 (0.23)	6.3 ± 1.52	8.57e49 (4.37)	...	5.88 (0.88)	7.48e49 (2.55)
041006	108 [22]	6.92e52 [0.7]	2.79 ± 0.41	8.18e49 (2.57)	...	2.62 (0.18)	7.25e49 (1.23)
050525	135 [8]	2.3e52 [0.3]	4.04 ± 0.8	5.73e49 (2.34)	...	4.04 (0.45)	5.72e49 (1.40)

Table 2. The rest frame peak energy $E'_{\rm p}$, the collimation corrected energy $E_{\gamma,\rm iso}$ are calculated with the parameters reported in Tab. 1. The semiaperture angle $\theta_{\rm j}$ is calculated with Eq. 1 in the case of an homogeneous medium and the collimation corrected energy E_γ is reported. We also report the values of $E_{\gamma,\rm n=3}$ assuming $n = 3$ cm^{-3} for the 4 GRBs which have a different estimate of n as reported in Tab. 1. In the case of a wind medium the semiaperture angle $\theta_{\rm j,w}$ (calculated by Eq. 6) and the corresponding $E_{\gamma,\rm w}$ are reported. When the errors in $E_{\rm p}$ ($E_{\gamma,\rm iso}$) are not given in the original reference, we assume the average error of 20% (11%) (values in square brackets), otherwise we list the originally reported error (in round brackets).

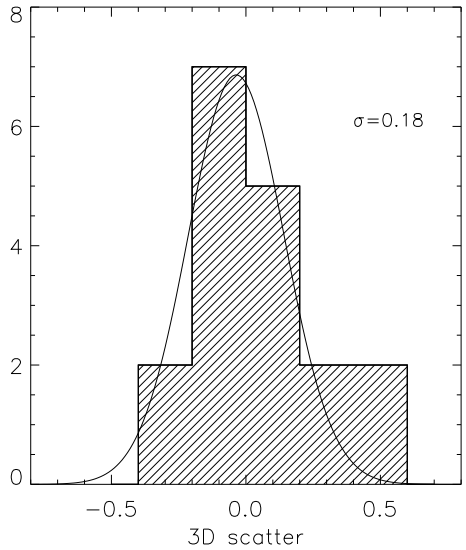

Fig. 2. Histogram of the scatter of the data points computed perpendicular to the best fit plane in the 3D space of Fig. 1. The solid line represents the gaussian fit which has a $\sigma = 0.18$.

this plane. The histogram of the scatter is reported in Fig.2 and, when fitted with a gaussian it has a $\sigma = 0.18$.

Comparing Eq. 4 with the original result of LZ05 we obtain a value of the $t'_{\rm j}$ exponent closer to unity, but still consistent with the value of LZ05 (which was also consistent with unity, due to the relatively larger uncertainty). As explained in the next section, a value equal to unity is crucial to make the LZ05 correlation and the Ghirlanda correlation mutually consistent.

We show in Fig. 3 the values of $E_{\gamma,\rm iso}$ calculated through Eq. 3 as a function of $E_{\gamma,\rm iso}$ calculated through the best fit of the correlation $E_{\gamma,\rm iso}(E'_{\rm p}, t'_{\rm j})$ found using our data and our method, and assuming a $\Omega_{\rm M} = 0.3$ and $h = \Omega_\Lambda = 0.7$ cosmology. As can be seen, there is a very good agreement.

It is interesting, in view of the discussion of the following sections, also to fit the $E_{\gamma,\rm iso}$, $E'_{\rm p}$ and $t'_{\rm j}$ correlation by forcing the slope of the $t'_{\rm j}$ to be –1. Fixing this slope we find $E_{\gamma,\rm iso}\, t'_{\rm j} \propto E'^{1.91\pm0.1}_{\rm p}$, with a reduced $\chi^2_r = 1.51$.

3.2. The updated Ghirlanda correlation

Using the same data listed in Tab. 1 we calculate the updated version of the Ghirlanda correlation. We find a Spearman correlation coefficient r_s =0.93 with a chance probability P=2.3×10^{-8}. We report in Fig. 4 the updated correlation with the 18 GRBs reported in Tab. 1.

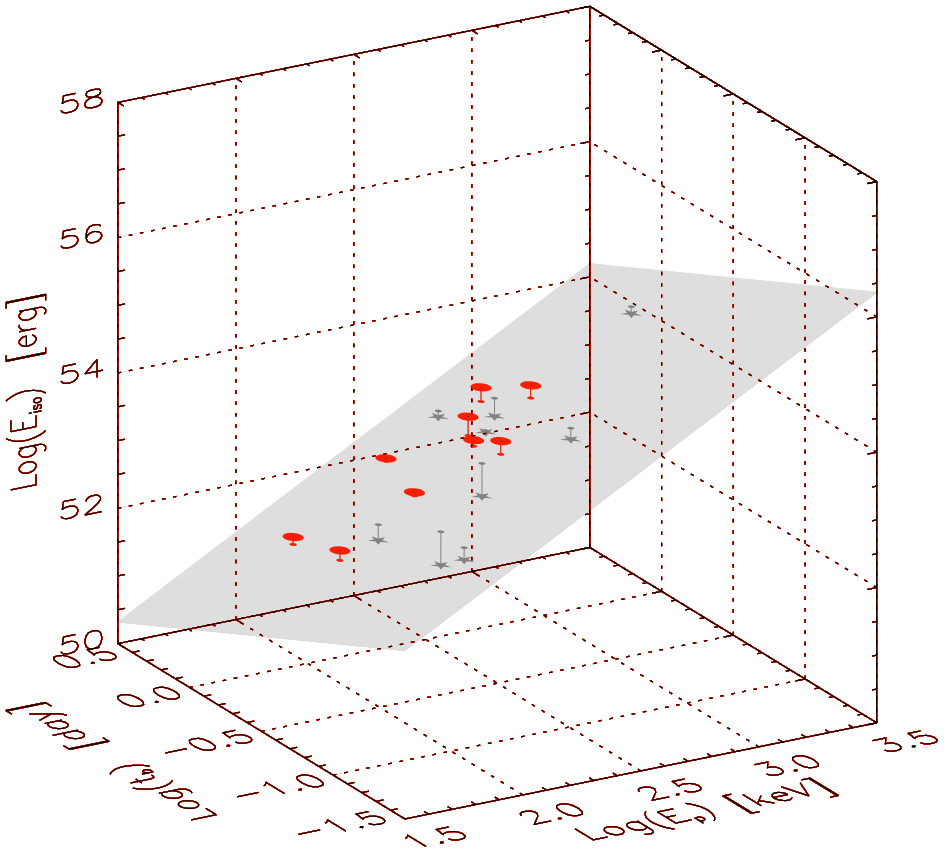

Fig. 1. Three dimensional representation of the $E_{\gamma,\rm iso}(E'_{\rm p}, t'_{\rm j})$ correlation. Data points are from Tab.2. The plane is the best fit to the data points as represented by Eq. 4 which has a reduced $\chi^2_{\rm r} = 1.49$. The red points lies above the best fit plane while the grey stars are below the plane. The height of each point with respect to the best fit plane is also shown.

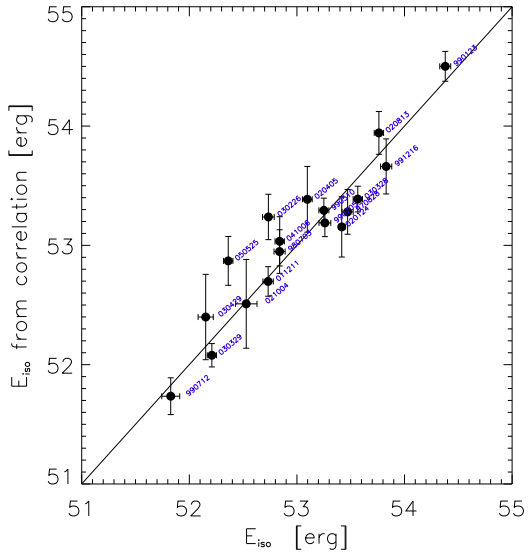

Fig. 3. $E_{\gamma,\rm iso}$ calculated through the best fit multidimensional correlation $E_{\gamma,\rm iso}(E'_{\rm p}, t'_{\rm j})$ (Eq. 4) as a function of the same quantity calculated through Eq. 3.

We fitted this correlation with a powerlaw model accounting for the errors on both variables, i.e. $E'_{\rm p}$ and E_γ (using the routine *fitexy* of Press et al. 1999). For $\Omega_{\rm M} = 0.3$, $\Omega_\Lambda = h = 0.7$ we find

$$\left(\frac{E'_{\rm p}}{100\,{\rm keV}}\right) = (2.79 \pm 0.15)\left(\frac{E_\gamma}{2.72\times10^{50}\,{\rm erg}}\right)^{0.69\pm0.04} \quad (5)$$

with a reduced $\chi^2_{\rm r} = 1.4$ for 16 degrees of freedom. The errors on its slope and normalization are calculated in the "barycenter" of $E'_{\rm p}$ and E_γ, where the slope and normalization errors are uncorrelated (Press et al. 1999). We also note that the simplest linear regression fit (i.e. without accounting for errors on the variables) gives a slope of 0.6 (dotted line in Fig. 4).

Fig. 4 shows the correlation for the 18 GRBs and its best fit represented by Eq. 5 (solid line). This updated correlation has a slope which is consistent with the original value found in GGL04. We also computed the scatter of the data points around this correlation (insert of Fig.4). This scatter is defined as the distance in the $\log E'_{\rm p} - \log E_\gamma$ plane of each data point from the best fit correlation. We find that if fitted with a gaussian its standard deviation is $\sigma = 0.1$, i.e. lower than the value originally found by GGL04.

For completeness, we also computed the Amati correlation with the 18 GRBs reported in Tab. 1. By weighting for the er-

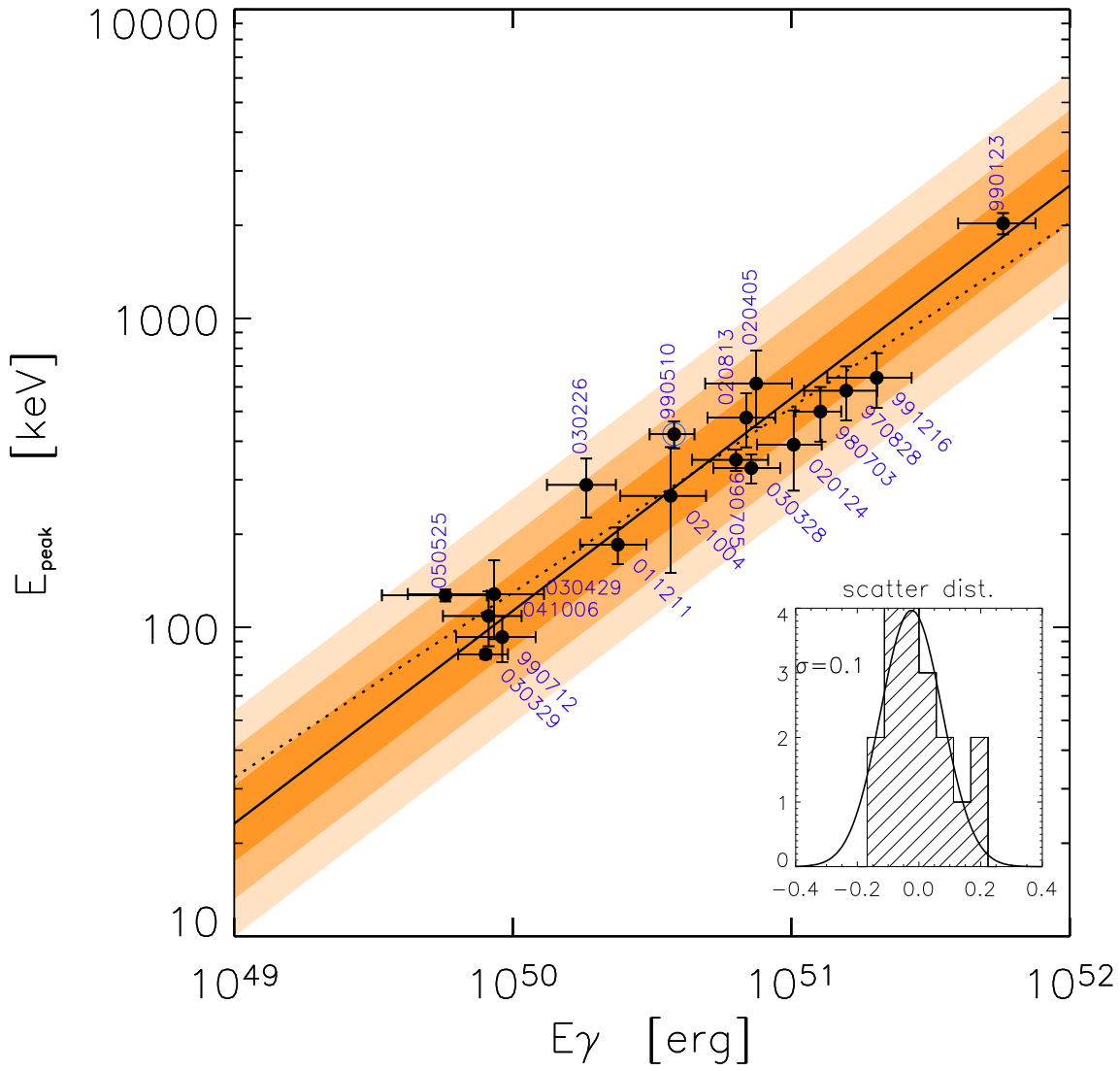

Fig. 4. The updated Ghirlanda correlation between the rest frame spectral peak energy $E'_{\rm p}$ and the collimation corrected energy E_γ as found with the 18 GRBs reported in Tab. 1. The solid line represents the best fit powerlaw model obtained accounting for the errors on both coordinates (Eq. 5) which has a reduced $\chi^2_{\rm r} = 1.4$ (16 dof) and a slope of 0.69±0.04. We also show the fit obtained with the simplest linear regression, i.e. without accounting for the errors on the coordinates (dotted line, slope equal to 0.6). The circled point represents GRB 990510 which alone contributes to the 27% of the total χ^2 of the fitted model. The names of the 18 GRBs are also reported. The shaded areas represent the regions corresponding to the 1, 2 and 3σ scatter around the best fit correlation. The *insert* reports the distribution (hatched histogram) of the scatter of the data points computed perpendicularly to the best correlation (solid line in main plot) and its gaussian fit (solid line in the insert) which has a $\sigma = 0.1$.

rors on $E_{\rm p}$ and $E_{\gamma,\rm iso}$, we find a relatively poor fit with a reduced $\chi^2_{\rm r} = 5.22$ and a best fit correlation $E_{\gamma,\rm iso} \propto E_{\rm p}^{0.57\pm0.02}$.

3.3. The Ghirlanda correlation in the case of a wind density profile

If the external medium is distributed with an r^{-2} density profile the semiaperture angle of the jet is related to the achromatic jet break through (Chevalier & Li 2000):

$$\theta_{\rm j,w} = 0.2016 \left(\frac{t_{\rm j,d}}{1+z}\right)^{1/4} \left(\frac{\eta_\gamma\, A_*}{E_{\gamma,\rm iso,52}}\right)^{1/4} \qquad (6)$$

where we assume $n(r) = Ar^{-2}$ and A_* is the value of A ($A = \dot{M}_{\rm w}/(4\pi v_{\rm w}) = 5 \times 10^{11} A_*$ g cm^{-1}) when setting the mass loss rate due to the wind $\dot{M}_{\rm w} = 10^{-5} M_\odot$ yr^{-1} and the wind velocity $v_{\rm w} = 10^3$ km s^{-1}, according to the Wolf–Rayet wind physical conditions.

In the wind case we use Eq. 6 to correct the isotropic energies $E_{\gamma,\rm iso}$ by the factor $(1 - \cos\theta_{\rm j,w})$. Given the few still uncertain estimates of the A_* parameter, we assume the typical value (i.e. $A_* = 1$) for all bursts neglecting for the moment the possible uncertainty on this parameter.

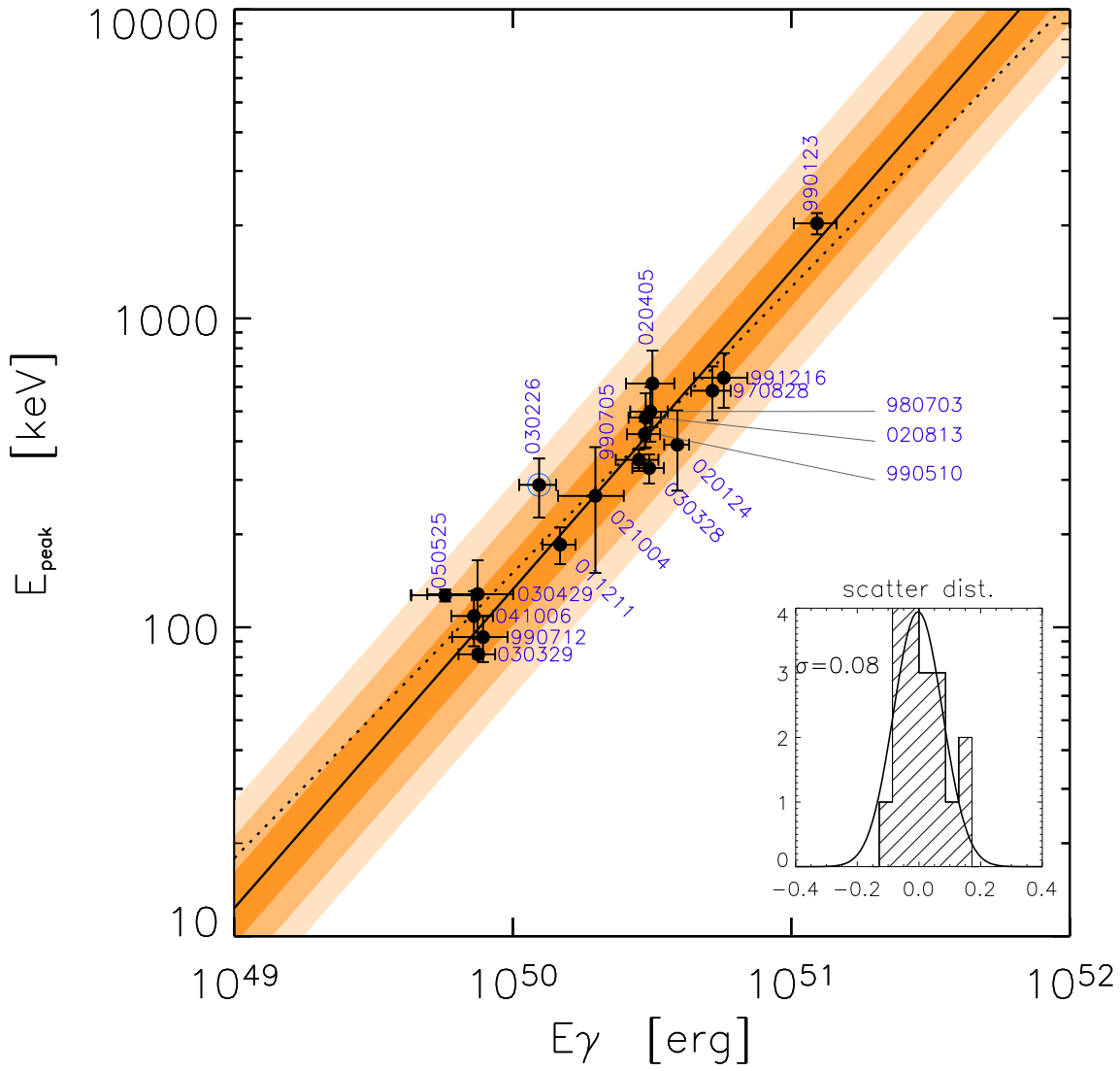

Fig. 5. The Ghirlanda correlation in the case of a wind profile of the external medium density as found with the 18 GRBs reported in Tab. 1 (col. 5). The values of E_γ are reported in Tab. 2. The solid line represents the best fit powerlaw model obtained accounting for the errors on both coordinates (Eq. 7) which has a reduced $\chi^2_{\rm r} = 1.125$ (16 dof) and a slope of 1.09±0.06. We also show the fit obtained with the simplest linear regression, i.e. without accounting for the errors on the coordinates (dotted line), which has a slope of 0.92. The circled point represents GRB 030326 which is giving the largest contribution (23%) to the best fit reduced χ^2. The shaded regions represent the 1, 2 and 3σ scatter around the best fit correlation. The names of the 18 GRBs are indicated. The *insert* reports the distribution (hatched histogram) of the scatter of the data points computed perpendicularly to the best correlation (solid line in the main plot) and its gaussian fit (solid line in the insert) which has a $\sigma = 0.08$.

In the wind case we find a correlation between $E'_{\rm p}$ and E_γ with a Spearman rank correlation coefficient $r_{\rm s} = 0.92$ ($P = 6.9 \times 10^{-8}$). The fit with a powerlaw model gives

$$\frac{E'_{\rm p}}{100\,{\rm keV}} = (3.0 \pm 0.16) \left(\frac{E_\gamma}{2.2\times10^{50}\,{\rm erg}}\right)^{1.03\pm0.06} \quad (7)$$

with a reduced $\chi^2_{\rm r} = 1.13$ for 16 dof (see Fig. 5). Note that the exponent of this new relation is entirely consistent with unity. The scatter of the points (insert of Fig. 5) around the best fit correlation is fitted by a gaussian with $\sigma = 0.08$.

Since we have no knowledge of the uncertainty associated with the ηA_* parameter entering in Eq. 6, we estimate that, for the assumed typical value $\eta A_* = 0.2$, an error $\sigma_{\eta A_*} \leq 20\%$ does not dominate the fit of the correlation (i.e. the reduced $\chi^2_{\rm r}$ is not much smaller than 1).

Since we have assumed that all the A_* values are equal and have no errors, the resulting χ^2_r of the wind case should be compared with the the case of homogeneous density assuming all the n values equal (we set $n = 3$ cm^{-3}) with no error (see Tab. 2). This case is shown in Fig. 7. In this case we obtain $\chi^2_r = 1.4$ to be compared with the $\chi^2_r = 1.125$ of the wind

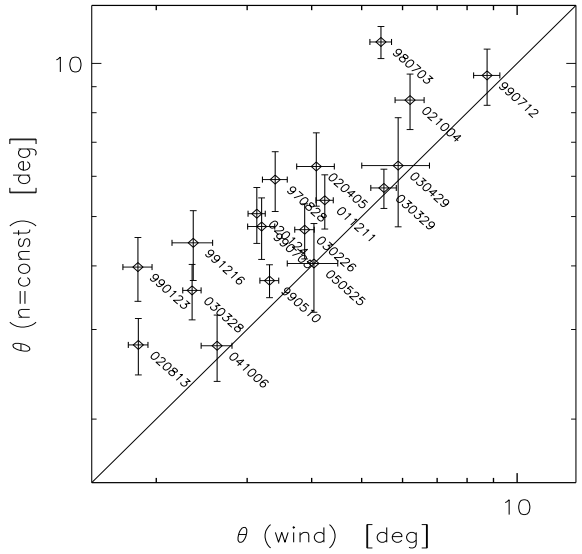

Fig. 6. Jet opening angles calculated for a homogeneous density profile (θ_j) and for a wind density profile ($\theta_{j,w}$) for the 18 GRBs reported in Tab. 2 (col. 4 and 7 respectively).

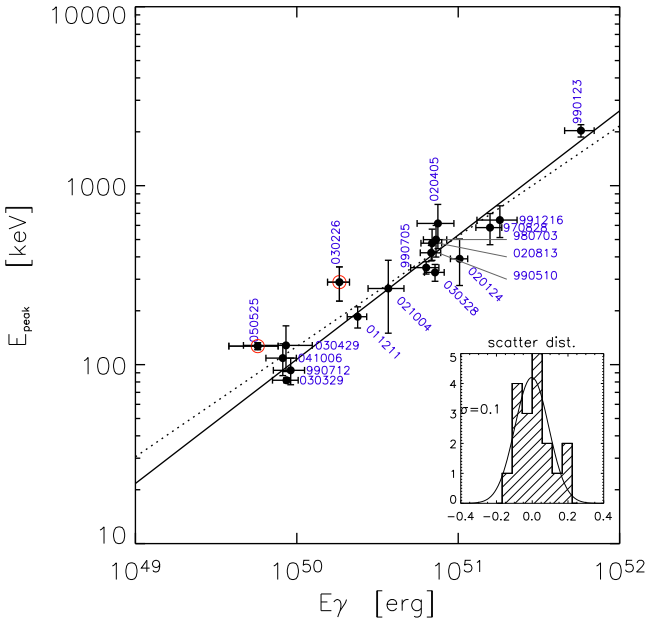

Fig. 7. The Ghirlanda correlation in the case of a homogeneous external medium assuming a universal value for the density, i.e n=3.0 without uncertainty, for comparison with the wind case. The solid line represent the best fit powerlaw model obtained accounting for the errors on both coordinates which has a reduced $\chi^2_{\rm r} = 1.4$ (16 dof) and a slope of 0.69 ± 0.04.

case. We conclude that the wind case gives a somewhat better χ^2_r and a somewhat tighter (smaller scatter) and a steeper correlation than the correlation found in the case of an homogeneous medium. Therefore, even if the wind density profile is not favored by the afterglow model we cannot discard it on the basis of the Ghirlanda relation.

The jet opening angles calculated in the case of a homogeneous medium or in the case of a wind density profile, for the sample of 18 GRBs, is reported in Fig. 6. The angle calculated in the wind case (Eq. 6) is sistematically smaller than in the homogeneous medium case (Eq. 1).

4. Consistency of the empirical correlation with the model dependent correlations

In this section we will demonstrate that the Ghirlanda correlation either assuming an homogeneous circumburst density or a wind density profile and the LZ05 correlation are mutually consistent. This allows us to make some interesting considerations on the scatter of the Ghirlanda correlations. The fact that the LZ05 and the Ghirlanda correlation are mutually consistent have been already pointed out by LZ05 (see also Xu 2005) in the case of an homogeneous medium.

For the simple analytical demonstration, we will consider a generic form of the LZ05 correlation, namely:

$$E_{\gamma,\rm iso} \propto E'^{A}_{\rm p} t'^{B}_{\rm j} \tag{8}$$

4.1. Homogeneous density

Adopting the standard fireball scenario, assuming a uniform jet and an homogeneous circumburst density distribution, the relation between $t'_{\rm j}$ and $\theta_{\rm j}$ is given by Eq. 1. Inserting it into Eq. 8 one obtains

$$E_{\gamma,\rm iso}\theta^2_{\rm j} \sim E_\gamma \propto E'^{3A/(3-B)}_{\rm p}\ \theta^{6(B+1)/(3-B)}_{\rm j} (n\eta_\gamma)^{-B/(3-B)} \tag{9}$$

where we have used the small angle approximation $(1 - \cos\theta_{\rm j}) \propto \theta^2_{\rm j}$. Eq. 9 relates five variables.

We have shown that the Ghirlanda correlation is characterized by a scatter $\sigma \sim 0.1$ (Sec. 3.2 and Fig. 4). If this scatter is entirely due to a dispersion of the $n\eta_\gamma$ values (and very likely also to the errors of measurements on the observables) and not to $\theta_{\rm j}$, we derive the condition $B = -1$ and Eq. 9 reduces to a relation between E_γ and $E'_{\rm p}$. This value of B is consistent with the value found from the fit of the LZ05 correlation (i.e. $B = -1.08 \pm 0.17$) with the 18 GRBs of our sample. If the exponent $B = -1$, then the slope g of the Ghirlanda correlation (i.e. $E'_{\rm p} \propto E^g_\gamma$) is related to the exponent A of the LZ05 correlation through $g = 4/(3A)$.

On the other extreme, if the scatter of the Ghirlanda correlation is completely due to $\theta_{\rm j}$ (and to the errors of measurements on the observables) we may still derive a range of allowance for the parameter B. We computed the standard deviation σ of the distribution of $\theta^{6(B+1)/(3-B)}_{\rm j}$ as a function of B. This is represented in Fig. 8 by the solid line. If we compare σ with the scatter of the Ghirlanda correlation (in the homogeneous density case - solid horizontal line in Fig. 8) we can find quite shallow constraints on $B \in (-1.3, -0.7)$.

Clearly, the intermediate case corresponds to both $n\eta_\gamma$ and $\theta_{\rm j}$ contributing to the scatter. If we consider the range of B as found by fitting the LZ05 correlation (Eq. 4), i.e. $B = -1.08 \pm 0.17$ (shaded region in Fig. 8) then the term $\theta^{6(B+1)/(3-B)}_{\rm j}$ can contribute at most for the $\sim$ 70% of the total scatter of the Ghirlanda correlation.

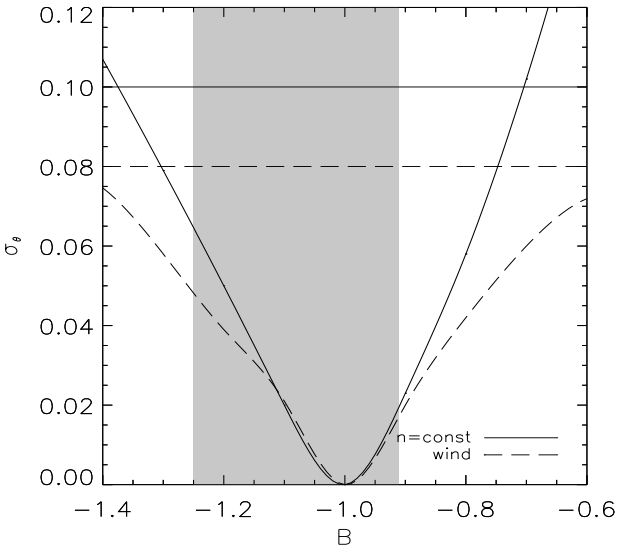

Fig. 8. Standard deviation of the distribution of $\theta^h(B)$ where $h(B)$ is given by Eq. 9 and Eq. 10 for the homogeneous (solid line and filled points) and wind density profile (long dashed line and open circles) as a function of the parameter B. The horizontal lines represent the scatter of the Ghirlanda correlation in the two scenarios (solid and long–dashed line respectively). The shaded region represents the (1σ) uncertainty on the parameter B (=-1.08 ± 0.17) found through the fit of the LZ05 correlation with the 18 GRBs.

4.2. Wind density profiles

If $t_{\rm j}$ is related to the semiaperture angle of the jet according to Eq. 6, the LZ05 correlation implies:

$$E_{\gamma,{\rm iso}}\theta^2_{\rm j,w} \sim E_\gamma \propto E'^{A/(1-B)}_{\rm p}\ \theta^{2(B+1)/(1-B)}_{\rm j}(n\eta_\gamma)^{-B/(1-B)} \quad (10)$$

For the same considerations reported in the previous section, we derive $B=-1$ if only the term $n\eta_\gamma$ contributes to the scatter of the Ghirlanda correlation in the wind density case (i.e. $\sigma\sim0.08$, Sec. 3.3 and Fig.5). In this case the relation between the Ghirlanda correlation and the LZ05 correlation implies that $E'_{\rm p}\propto E^{2/A}_\gamma$.

If we consider that the scatter of the Ghirlanda correlation (long dashed horizontal line in Fig. 8) is entirely due to the term $\theta^{2(B+1)/(1-B)}_{\rm j}$ we can derive even shallower (with respect to the homogeneous case) constraints on the parameter $B\in(-1.45,-0.65)$ (Fig. 8 - long dashed curve). Again in the intermediate case, i.e. both $n\eta_\gamma$ and $\theta_{\rm j}$ contributing to the scatter of the Ghirlanda correlation, if we assume the range of possible values of B resulting from the fit of the LZ05 correlation than the term $\theta^{2(B+1)/(1-B)}_{\rm j}$ contributes at most for the $\sim$60% to the scatter observed in the Ghirlanda correlation.

5. The Ghirlanda correlation in the comoving frame

The values of $E'_{\rm p}$ and E_γ we derive are the ones seen in the GRB rest frame but not in the fireball comoving frame.

In the simplest and standard scenario, which assumes that the observer's line of sight is within the jet opening angle and that the jet is homogeneous, $E_{\rm p}$ and E_γ are both boosted by a factor $\sim2\Gamma$, i.e. the blueshift of the photons.

Then the comoving $E^{\rm com}_\gamma = E_\gamma/(2\Gamma)$ and $E^{\rm com}_{\rm p} = E'_{\rm p}/(2\Gamma)$. Here Γ is the bulk Lorentz factor of the fireball emitting the prompt radiation.

We then exploit the fact that we see a very tight correlation (in the rest, but not comoving, frame) to pose some limits on the physics (i.e. the dynamics and the radiation process) of bursts.

Let us assume that the most general Ghirlanda correlation described by a generic power law, i.e. $E'_{\rm p}\propto E^g_\gamma$, which can then represents the correlation for both the homogeneous and wind density profiles. In the comoving frame, each point must be corrected by the bulk Lorentz factor of that burst. If these bulk Lorentz factors are uncorrelated with E_γ or $E'_{\rm p}$, then in the comoving frame the correlation is destroyed. It would then seem very strange that two quantities that are not correlated in the comoving frame appear to be correlated in the rest frame. We then are obliged to assume that Γ is a function of E_γ (or, equivalently, of $E^{\rm com}_\gamma$). To this aim, let assume a simple power law relation:

$$\Gamma\ \propto\ \left(E^{\rm com}_\gamma\right)^x; \qquad \Gamma\ \propto\ E^{x/(1+x)}_\gamma; \quad (11)$$

The two relations above are equivalent. In the comoving frame we have:

$$E^{\rm com}_{\rm p}\ \propto\ \left(E^{\rm com}_\gamma\right)^{xg-x+g} \quad (12)$$

Note that:

- If $x=0$ (i.e. all bursts have the same Lorentz factor) then the slope in the comoving and in the rest frame is the same;
- If $g=1$ (i.e. wind case), the correlation is linear also in the comoving frame;
- The exponent x can be thought as determined by a particular dynamical model of the fireball. Once x is fixed, then the exponent $(xg-x+g)$ appearing in Eq. 12 should be explained by the radiative process. Viceversa, if we have reason to fix, through a specific radiation model, the exponent of Eq. 12, then we have information on the dynamics of the fireball.

We stress the fact that for the wind case (i.e. $g=1$) we obtain *a linear relation, whose slope is therefore "Lorentz invariant"*. This of course would greatly help to explain the existence of the Ghirlanda correlation, since one of the main parameters, the bulk Lorentz factors, does not enter to determine it. In other words, in the case of the wind, the explanation of the correlation should be found in the radiation process only, independently of the dynamics.

6. Discussion

We have shown that the model–independent correlation recently found by LZ05 between the isotropic emitted energy $E_{\gamma,{\rm iso}}$, the rest frame peak energy $E'_{\rm p}$ and the jet break time $t'_{\rm j}$, calculated in the rest frame, is equivalent to the Ghirlanda correlation.

We have also shown that an even tighter correlation is found assuming that the circumburst density is distributed with an r^{-2} wind profile. Remarkably enough, this Ghirlanda–wind correlation is linear, and this slope is independent of the Lorentz correction needed to find out the correlation in the comoving frame.

We are aware that the wind–like distribution of the circumburst medium is not favored by the existing afterglow modeling, but the advantage of having a linear Ghirlanda correlation is so great to justify a deeper analysis, to see if there can be some neglected effects which might be able to hide the presence of the wind. This is however out of the scope of the present paper, and we defer this issue to future studies. Here we only mention that one of the main assumption of the afterglow modeling might be particularly suspect, namely the hypothesis that the equipartition parameters ϵ_B and ϵ_e (i.e. the fraction of the dissipated energy converted in the magnetic field and in the electron energy, respectively) are kept fixed during the entire afterglow phase (while they have very different values from burst to burst). For instance, in the case of $\epsilon_B \propto \Gamma^{-\lambda}$, the synchrotron cooling is enhanced at later times with respect to the case of a constant ϵ_B, and this makes the light curve of a fireball moving in a wind circumburst environment to mimic the evolution of a fireball expanding in a uniform medium with a constant ϵ_B (the two cases becomes almost indistinguishable for $\lambda = 2$). Consider also that all the pieces of evidence we have up to now point towards a massive stellar progenitor of GRBs, and it is difficult to understand why there is no sign of winds around such massive stars. The fact that ϵ_B changes (as long as its evolution law does not change), does produces a different (with respect to a not–evolving ϵ_B) decay law of the afterglow flux, but with no breaks. Therefore in this case ϵ_B does not enter in the estimate of the jet opening angle (as long as we are in the adiabatic regime).

One interesting developement (Ghirlanda et al. 2005a) of having found a somewhat tighter and steeper Ghirlanda correlation in the wind density case (with respect to the homogenous case) is to use it to constrain the cosmological prameters similarly to what already done through the Ghirlanda correlation in the homogeneous case (Ghirlanda et al. 2004a; Firmani et al. 2005).

As pointed out by Ghirlanda, Ghisellini & Firmani (2005), the existence of the Ghirlanda correlation explains the Amati correlation between $E_{\gamma\rm iso}$ and $E'_{\rm p}$ (Amati et al. 2002, Ghirlanda, Ghisellini & Lazzati 2004), and in particular explains why the Amati correlation has a much larger scatter than the Ghirlanda correlation. In fact if GRBs are characterized by a distribution of semiaperture angles for each value of $E'_{\rm p}$, then one sees a variety of $E_{\gamma,\rm iso}$–values for each value of $E'_{\rm p}$. If the (observed) distribution of aperture angles turns out to have a preferred value, where it peaks, then this naturally produces a correlation in the $E'_{\rm p}$–$E_{\gamma,\rm iso}$ plane. Furthermore, it is conceivable that the bursts with spectroscopically measured redshifts are the brightest, hence with the smallest aperture angles (for a given redshift), hence lying at the large $E_{\gamma,\rm iso}$ end of the real distribution. We have evidence that this is just what is happening (Ghirlanda, Ghisellini & Firmani 2005).

Therefore the Amati correlation can be easily explained by assuming the existence of i) the Ghirlanda correlation and ii) the existence of a (peaked) distribution of jet aperture angles. Thus what remains to be explained is the Ghirlanda correlation itself which is relating the intrinsic collimation corrected quantities. We have pointed out that there might be a difference between the apparent and the comoving Ghirlanda correlation, and from the theoretical point of view it is the comoving one that should be explained. As Rees & Meszaros (2005) pointed out, a tight relation between the peak energy of the spectrum and the total emitted energy reminds of a thermal process, where the peak energy is a measure of a temperature. It is in this direction that we plan to investigate in the future.

Finally, let us comment, regarding the linear, wind–like, Ghirlanda correlation, which implies that the number of "relevant" photons (the ones with energies close to $E'_{\rm p}$) is constant in all bursts, and approximately equal to $N_\gamma = 10^{57}$, a number (coincidentally?) close to the number of baryons in one solar mass. In the "standard" scenario, in which the primary energy is injected close to the putative newly born black hole in a high entropy form, the requirement of a fixed number of photons N_γ translates in the requirement that the product of the injected energy E and the typical size of the injection region R is constant. This can be seen in a simple way by noting that $aT^4R^3/(kT) \sim N_\gamma$, where T is the temperature of the initial blackbody. Since $E \sim kTN_\gamma$, one arrives to $ER \propto N_\gamma^{4/3}$ =const. In the framework of the standard scenario, in the absence of additional injection of energy, the number of photons is conserved during the acceleration and the coasting phase. Then, when the fireball becomes transparent, this blackbody–like component has a fixed number of photons. But bursts with different baryon loading would become transparent at different times, meaning that different fractions of the energy initially contained in the radiation field have survived to the conversion to the bulk kinetic energy. This means different efficiency factors η_γ. And this is contrary to one of the main assumptions leading to the construction of the Ghirlanda correlation itself, which has been derived assuming the same η_γ for all bursts.

If some extra dissipation of kinetic energy occurs after the acceleration phase, before the transparency radius, and the main radiation process is Comptonization, then we can reconvert part of the kinetic energy into radiation energy leaving the number of photons unaltered. The available time to do it will be proportional to the transparency radius, so we have the positive feedback that sources which becomes transparent later (i.e. more baryon loaded, and hence with a radiation content which will be less energetic), have more possibilities to be re–energized by this putative dissipation (Rees & Meszaros 2005). This positive feedback can narrow the range of radiative efficiencies. In any case, we face the problem to explain why bursts with the same number of photons have different total energies.

Apart from these theoretical considerations, there might be an "observational" way to see if the real E_γ–$E'_{\rm p}$ is wind–like or constant density–like. Assume in fact that there is indeed a correlation between $E_{\rm p}$ and E_γ and suppose that it will be possible to estimate the bulk Lorentz factor of the fireball during

the emission of the prompt (that should be roughly equal to the bulk Lorentz factor of the very early afterglow, and controls the time at which there is the peak flux of the afterglow itself). Preliminary attempts to estimate it have already been done by e.g. Soderberg & Ramirez–Ruiz (2002) for GRB 990123. Then, if by "de–beaming" the E_γ and $E'_{\rm p}$ values (i.e. computing them in the comoving frame) in the case of an homogeneous density one finds an equally tight correlation, this would strongly point in favor of the validity of the homogeneous density hypothesis. Perhaps more importantly, one will also find the relation between Γ and $E_\gamma^{\rm com}$. On the contrary, if the de–beamed quantities (calculated in the case of an homogeneous density) do not correlate, this will strongly argue in favor of the wind hypothesis (in such a case the de–beamed quantities still correlate).

Acknowledgements. We thank the referee Amir Levinson for his valuable comments. We thank Annalisa Celotti and Davide Lazzati for discussions. The Italian MIUR and INAF are thanked for founding (Cofin grant 2003020775_002).

References

Amati, L., Frontera, F., Vietri, M., et al. 2000, Science, 290, 953
Amati, L., Frontera, F., Tavani, M., et al. 2002, A&A, 390, 81
Amati, L. 2004, astro-ph/0405318
Andersen, M.I., Masi, G., Jensen, B.L., & Hjorth, J. 2003, GCN Circ., 1993
Atteia, J.-L., Kawai. N., Vanderspek, R., et al. 2005, ApJ, 626, 292
Atteia, J.-L., 2003, A&A, 407, L1
Barraud, C., Olive, J.-F., Lestrade, J.P., et al. 2003, A&A, 400, 1021
Barth, A. J., Sari, R., Cohen, M.H., et al. 2003, ApJ, 584, L47
Berger, E., Kulkarni, S.R., Bloom, J.S., et al. 2002, ApJ, 581, 981
Berger, E., Kulkarni, S.R., Pooley, G., et al. 2003, Nature, 426, 154
Bjornsson, G., Hjorth, J., Jakobsson, P., Christensen, L., & Holland, S. 2001, ApJ, 552, L121
Bloom, J. S., Frail, D. A., & Kulkarni, S. R. 2003, ApJ, 594, 674
Blustin, A.J., Band, D., Barthelmy, S., et al. 2005, astro-ph/0507515
Chevalier, R. A. & Li, Z. Y., 2000, ApJ, 536, 195
Della Valle, M., Malesani, D., Benetti, S., et al., 2003, A&A, 406, L33
Djorgovsky, S.G., Kulkarni, S.R., Bloom, J.S., Goodrich, R., Frail, D.A., Piro, L., & Palazzi, E. 1998, ApJ, 508, L17
Djorgovsky, S.G., Frail, D.A., Kulkarni, S.R., Bloom, J.S., Odewahn, S.C., & Diercks, A. 2001, ApJ, 562, 654
Eichler, D. & Levinson, A., 2004, ApJ, 614, L13x
Firmani, C., Ghisellini, G., Ghirlanda, G., Avila–Reese, V., 2005, MNRAS, 630, L1
Foley, R.J., Chen, H.-W., Bloom, J., & Prochaska, J.X. 2005, GCN Circ, 3483
Frail D. A., Kulkarni S. R., Sari R., et al., 2001, ApJ, 562, L55
Frail, D.A., Soderberg, A.M., Kulkarni, S.R., Berger, E., Yost, S., Fox, D.W.,& Harrison, F.A., 2005, ApJ, 619, 994
Ghirlanda, G., Ghisellini, G. & Lazzati, D. 2004, ApJ, 616, 331
Ghirlanda, G., Ghisellini, G., Lazzati, D. & Firmani, C., 2004a, ApJ, 613, L13
Ghirlanda, G., Ghisellini, G. & Firmani, C. 2005, MNRAS, 361, L10
Ghirlanda, G. et al., 2005a, to be submitted
Greiner, J., Guenther, E., Klose, S., & Schwarz, R. 2003a, GCN Circ., 1886
Greiner, J., Peimbert, M., Estaban, C., et al. 2003b, GCN Circ., 2020
Hjorth, J., Andersen, M.I., Cairos, L.M., et al. 1999, GCN Circ., 219
Hjorth, J., Moller, P., Gorosabel, J., et al. 2003, ApJ, 597, 699
Holland, S.T., Weidinger, M., Fynbo, J.P.U., et al. 2003, AJ, 125, 2291
Holland, S.T., Bersier D., Bloom J. S., et al., 2004, AJ, 128, 1955
Israel, G., Marconi, G., Covino, S., et al. 1999, A&A, 384, L5
Jakobsson, S.P., Hjorth, J., Fynbo, J.P.U., et al. 2003, A&A, 408, 941
Jakobsson, P., Hjorth, J., Fynbo, J.P.U., et al. 2004, A&A, 427, 785
Jimenez, R., Band, D. & Piran, T. 2001, ApJ, 561, 171
Klose, S., Greiner, J., Rau, A., et al. 2004, AJ, 128, 1942
Klotz, A., Boer, M., Atteia, J. -L., et al., 2005, A&A, 439, L35
Kulkarni, S.R., Djorgovsky, S.G., Odewahn, S.C., et al. 1999, Nature, 398, 389
Levinson, A. & Eichler, D., 2005, ApJ, 629, L13
Liang, E. & Zhang, B., 2005, ApJ, in press (astro–ph/0504404)
Mirabal, N., Bonfield, D., Schawinski, K., 2005, GCN, 3488
Moller, P., Fynbo, J.P.U., Hjorth, J., et al. 2002, A&A, 396, L21
Panaitescu, A. & Kumar, P., 2000, ApJ, 543, 66
Panaitescu, A. & Kumar, P., 2001, ApJ, 560, L49
Panaitescu, A. & Kumar, P., 2002, ApJ, 571, 779
Press, W.H. et al. 1999, *Numerical Recipes in C*, Cambridge University Press, 661
Price, P.A., Kulkarni, S.R., Berger, E., et al. 2003, ApJ, 589, 838
Rees, M.J. & Meszaros, P., 2005, ApJ, 628, 847
Rol, E., Vreeswijk, P., & Jaunsen, A. 2003, GCN Circ., 1981
Sakamoto, T., Lamb, D.Q., Kawai, N., et al. 2005, ApJ, 629, 311
Sari R. 1999, ApJ, 519, L17
Soderberg, A.M. & Ramirez–Ruiz, E., 2002, MNRAS, 330, L24
Stanek, K.Z., Garnavich, P.M., Nutzman, P.A., et al. 2005, ApJ, 626, L5
Toma K., Yamazaki R. & Nakamura T., 2005, ApJ, 620, 835
Vanderspek, R., Sakamoto, T., Barraud, C., et al. 2004, ApJ, 617, 1251
Vreeswijk, P.M., Rol, E., Hjorth, J., et al. 1999, GCN Circ., 496
Vreeswijk, P.M., Fruchter, A., Kaper, L., et al. 2001, ApJ, 546, 672
Weidinger, M., Fynbo, J.P.U., Hjorth, J., Gorosabel, J., Klose, S., & Tanvir, N. 2003, GCN Circ., 2215
Xu, D., subm. to ApJ (astro–ph/0504052)
Yamazaki, R., Ioka, K. & Nakamura, T., 2004, ApJ, 606, L33